



This open access document is posted as a preprint in the Beilstein Archives at <https://doi.org/10.3762/bxiv.2024.29.v1> and is considered to be an early communication for feedback before peer review. Before citing this document, please check if a final, peer-reviewed version has been published.

This document is not formatted, has not undergone copyediting or typesetting, and may contain errors, unsubstantiated scientific claims or preliminary data.

**Preprint Title** Signal generation in dynamic interferometric displacement detection

**Authors** Knarik Khachatryan, Simon Anter, Michael Reichling and Alexander von Schmidsfeld

**Publication Date** 08 Mai 2024

**Article Type** Full Research Paper

**ORCID® IDs** Knarik Khachatryan - <https://orcid.org/0009-0006-8403-7274>; Simon Anter - <https://orcid.org/0009-0005-9649-6622>; Michael Reichling - <https://orcid.org/0000-0003-3186-9000>



License and Terms: This document is copyright 2024 the Author(s); licensee Beilstein-Institut.

This is an open access work under the terms of the Creative Commons Attribution License (<https://creativecommons.org/licenses/by/4.0>). Please note that the reuse, redistribution and reproduction in particular requires that the author(s) and source are credited and that individual graphics may be subject to special legal provisions.

The license is subject to the Beilstein Archives terms and conditions: <https://www.beilstein-archives.org/xiv/terms>.

The definitive version of this work can be found at <https://doi.org/10.3762/bxiv.2024.29.v1>

# 1 **Signal generation in dynamic interferometric displacement detection**

2 Knarik Khachatryan\*<sup>1</sup>, Simon Anter, Michael Reichling\* and Alexander von Schmidsfeld

3 Address: <sup>1</sup>Institut für Physik, Universität Osnabrück, Barbarastr. 7, 49076 Osnabrück, Germany

4 Email: Knarik Khachatryan - knarik.khachatryan@uos.de; Michael Reichling - reichling@uos.de

5 \* Corresponding author

## 6 **Abstract**

7 Laser interferometry is a well-established and widely used technique for precise displacement mea-  
8 surements. In a non-contact atomic force microscope (NC-AFM) it facilitates the force measure-  
9 ment by recording the periodic displacement of an oscillating micro-cantilever. To understand sig-  
10 nal generation in a NC-AFM based on a Michelson-type interferometer, we evaluate the non-linear  
11 response of the interferometer to the harmonic displacement of the cantilever in the time domain.  
12 As the interferometer signal is limited in amplitude due to the spatial periodicity of the interfer-  
13 ometer light field, an increasing cantilever oscillation amplitude creates an output signal with an  
14 increasingly complex temporal structure. By the fit of a model to the measured time-domain signal,  
15 all parameters governing the interferometric displacement signal can precisely be determined. It is  
16 demonstrated, that such an analysis specifically allows the calibration of the cantilever oscillation  
17 amplitude with 0.15% accuracy.

## 18 **Keywords**

19 force microscopy, NC-AFM, displacement detection, interferometer signal, amplitude calibration

## 20 **Introduction**

21 Optical interferometry is a reliable technique utilizing light waves to measure distance and dis-  
22 placement with high precision [1,2]. With the light wavelength, as the length standard, a highly

23 stable interferometer can detect displacements with an accuracy far beyond nanometer resolution  
 24 [3], where the final physical limit is set by the photon emission statistics of the light source [4]. In  
 25 non-contact atomic force microscopy (NC-AFM) interferometry is used to measure the periodic  
 26 displacement of a (quasi) harmonically oscillating micro-cantilever, acting as one mirror of the in-  
 27 terferometer, while the second mirror is the even surface of an optical fiber delivering the light to  
 28 the micro-cantilever [5-10].

29 As illustrated in Fig.1, interference occurs in the optical fiber between the light beams, reflected  
 30 from the fiber end (reference beam) and the cantilever (cavity beam), respectively, creating a stand-  
 31 ing wave pattern in the fiber with a spatial periodicity given by the light wavelength  $\lambda$  and a phase  
 32  $\phi$  determined by the distance  $d$  between the fiber end and the cantilever. Any variation in  $d$  results  
 33 in a variation of the intensity  $I_M$  recorded by a detector placed at a fixed distance to the fiber end  
 34 [11]. In our setup, there is a strong imbalance of reflectivity coefficients between fiber ( $r_f$ ) and  
 35 cantilever ( $r_c$ ) yielding an interferometer signal with a large constant intensity  $\bar{I}_M$  and a small in-  
 36 tensity variation upon a change in  $d$ .

37 As light exits the fiber with a certain divergence and the fiber core has a small diameter (4 $\mu$ m),  
 38 there is a finite number of multiple reflections between the cantilever and fiber. At large distance  
 39  $d$ , this number is small and the setup basically acts as a Michelson interferometer. Experiments re-  
 40 ported here are performed with the dielectric/vacuum interface of the fiber end acting as the first  
 41 mirror and a metal-coated silicon cantilever as the second mirror. We keep the fiber-cantilever dis-  
 42 tance  $d$  always large enough to work in the Michelson regime characterised by a low Fabry-Pérot  
 43 enhancement factor [12].

44 To obtain a model description of the interference light intensity at the detector, we virtually place  
 45 the detector inside the fiber at its end and consider the electric field of the incident light beam  $E_{inc}$   
 46 at this position, the electric field of the reference light beam  $E_{ref} = r_f E_{inc}$  and the electric field  
 47 reflected from the cantilever and entering the fiber  $E_{cav} = t_f^2 r_c s_{loss}(2d) e^{i(\phi(d)+\pi)} E_{inc}$ . As interfer-  
 48 ence occurs in the fiber, the transmissivity can be represented as  $T_f = t_f^2$  and it is independent of  
 49 the polarisation for (quasi) normal incidence. The a priori unknown function  $s_{loss}(2d)$  describes

50 the loss of light in the gap between the fiber end and the cantilever due to beam divergence. The  
 51 spatial variation of the electric field strength due to interference is governed by the path difference  
 52  $2d$  determining the phase of the interference electric fields  $\phi(d) = 2\pi\frac{2d}{\lambda}$ .

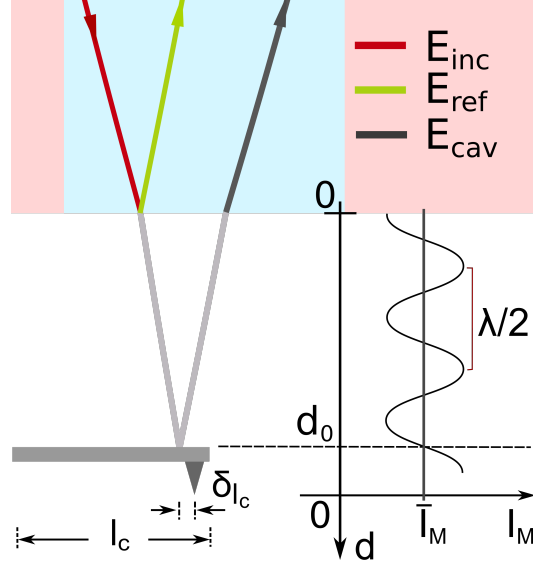


**Figure 1:** Michelson type interferometer formed by an optical fiber end and a micro-cantilever. The graph and physical quantities are explained in the text.

53 Linear superposition of reference and cavity beams yields as the intensity measured by the detector

$$54 \quad I_M = [E_{inc}(r_f - T_f r_c S_{loss}(2d)e^{i\phi(d)})]^2. \quad (1)$$

55 By introducing the incoming light intensity  $I_0 = \frac{1}{2}c\epsilon_0 E_{inc}^2$ , where  $c$  is the speed of light in vacuum  
 56 and  $\epsilon_0$  is the vacuum permittivity, and the reflectivities  $R_f = (r_f)^2$ ,  $R_c = (r_c)^2$  and cavity loss  
 57  $S_{loss}(2d) = (s_{loss}(2d))^2$ , Eq. (1) is transformed into

$$58 \quad I_M(d) = I_0 \left[ R_f + (1 - R_f)^2 R_c S_{loss}(2d) - 2\sqrt{R_f R_c} (1 - R_f) \cdot \sqrt{S_{loss}(2d)} \cos\left(2\pi\frac{2d}{\lambda}\right) \right], \quad (2)$$

59 where the transmissivity  $T_f$  is substituted by  $1 - R_f$  representing the law of energy conservation. A  
 60 sketch of the intensity measured at the detector of the Michelson type interferometer  $I_M$  as a func-  
 61 tion of  $d$  is shown in the right part of Fig. 1, where the distance dependence  $S_{loss}(2d)$  has been ne-

62 glected. The interference pattern has a periodicity of  $\lambda/2$ , while the curve crosses the mean value  
63 of intensity  $\bar{I}_M$  every  $n\lambda/4$ , where  $n$  is a positive integer. Usually, the interferometer is adjusted to  
64 positions  $d_0 = m\lambda/8$ , where  $m$  is an odd integer representing inflection points of the interference  
65 curve, where the slope of  $I_M(d)$  is a maximum. Such an adjustment facilitates a most sensitive  
66 displacement detection. Note, that it is not possible to adjust the interferometer to  $d_0$  with a small  
67 number  $m$  due to limitations in positioning the fiber end face parallel to the cantilever surface.  
68 Upon excitation, the freely oscillating cantilever exhibits a harmonic displacement  $q(t)$  as a func-  
69 tion of time. If a tip-surface force  $F_{ts}$  is present, this will introduce a slight anharmonicity and  
70 there will be a static displacement  $q_s$ [13]. Within the harmonic approximation, that is well justi-  
71 fied for small tip-surface forces, the cantilever displacement is [13]

$$72 \quad q(t) = q_s + A \sin(2\pi f_{exc}t), \quad (3)$$

73 where  $A$  is the cantilever oscillation amplitude and  $f_{exc}$  is the excitation frequency kept at the reso-  
74 nance frequency of the cantilever for frequency modulation NC-AFM. Further taking into account  
75 that the interferometer may be misaligned by the amount  $d_{err}$ , we find for the time-dependent fiber-  
76 cantilever distance

$$77 \quad d(t) = d_0 + d_{err} - q(t) = d_0 + d_{err} - q_s - A \cdot \sin(2\pi f_{exc}t). \quad (4)$$

78 Combining Eqs. (2) and (4) yield the time dependence of the light intensity at the detector. As the  
79 detector measures the total incident light power, we introduce the circular illuminated effective area  
80 of the detector  $\pi r_{eff}^2$ . The factor  $f_{loss}$  takes all optical losses into account occurring in the fiber de-  
81 livering the light to the cantilever and to the detector. The time domain signal of the interferometer  
82 is then given as

$$P_M(t) = f_{loss} \pi r_{eff}^2 I_0 \left[ R_f + (1 - R_f)^2 R_c S_{loss}(2d(t)) + 2\sqrt{R_f R_c} (1 - R_f) \sqrt{S_{loss}(2d(t))} \cdot \sin \left( \frac{4\pi}{\lambda} (d_0 + d_{err} - q_s - A \cdot \sin(2\pi f_{exc}t)) - \frac{\pi}{2} \right) \right].$$

84 Analysing the result, we find that the characteristics of the oscillatory part of  $P_M$  is determined by  
 85 the ratio between the cantilever oscillation amplitude  $A$  and the wavelength  $\lambda$ . For  $A \ll \lambda/8$ , the  
 86 detector signal oscillates quasi-sinusoidal with the fundamental frequency  $f_{exc}$ , for  $A \approx \lambda/8$ , the  
 87 signal is a strongly distorted sine and when increasing the amplitude further, the signal is more and  
 88 more dominated by higher frequency oscillations. Exemplary waveforms are shown schematically  
 89 in Fig. 4.

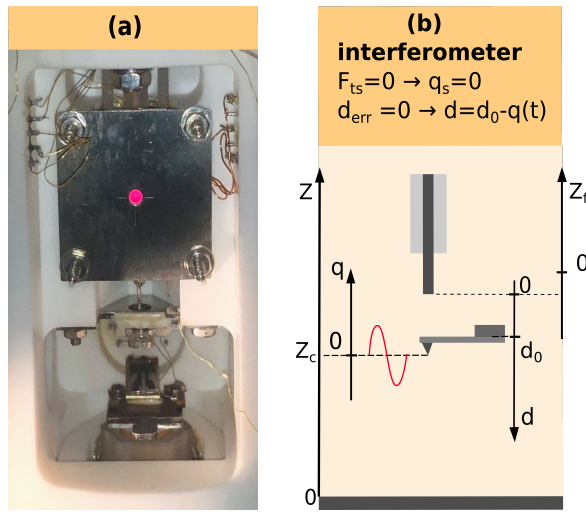


**Figure 2:** (a) Photo of the AFM scanhead showing the fiber and fiber coarse approach assembly (top), the removable cantilever holder (middle) and the sample plate with a mirror inserted for inspection purposes (bottom). (b) Coordinates for fiber movement  $z_f$  and cantilever displacement  $d$  in relation to the tip-sample coordinate  $z$  [14]. The cantilever is shown in its relaxed position where  $q_s = 0$  and  $A \sin(2\pi f_{exc}t) = 0$ . Note, that the origin of the  $d$ -axis is fixed at the fiber end.

## 90 Results and Discussion

91 The interferometer used for our experiments is part of a home-built NC-AFM, operated under ultra-  
 92 high vacuum (UHV) conditions [15]. The cantilever is a highly reflective ( $R_c = 0.81$ ) aluminum-  
 93 coated silicon micro-cantilever (type NCHR, NanoWorld AG, Neuchâtel, Switzerland) with an  
 94 eigenfrequency of  $f_0 = 169.67622$  kHz and a quality factor of  $Q = 9000$ . After transfer of the  
 95 cantilever, that is glued to a cantilever holder, the cantilever is mechanically firmly attached to the

96 AFM scan head, while the optical fiber and the sample are approached to the cantilever and the tip  
97 by piezoelectric motors for coarse motion [16] and tube piezos [17] for fine positioning in all direc-  
98 tions. The scanhead with cantilever, sample support, and the respective motion elements is shown  
99 in Fig. 2(a). The fine adjustment of  $d$  is accomplished by the fiber tube piezo, which is in its re-  
100 laxed position for  $z_f = 0$ , according to the coordinate system given in Fig. 2(b). Note, that the tube  
101 piezo allows for an adjustment of  $d$  with high accuracy, however, the absolute distance between the  
102 fiber end and the cantilever can practically neither be set nor measured. The interferometer is ad-  
103 justed to a fairly large value  $d_0$  to assure operation in the Michelson mode resulting in a detector  
104 signal  $I_M$  that is much smaller than what could be obtained by working in the Fabry-Pérot mode  
105 [12].

106 A temperature and intensity stabilized laser diode light source (type 48TA-1-42037, Schäfter +  
107 Kirchhoff GmbH, Hamburg, Germany) operating at a vacuum wavelength of  $\lambda = 796.42$  nm deliv-  
108 ers the light to the cantilever via a single-mode optical fiber (type Hi780, Corning Inc., New York,  
109 USA) with a core having a refractive index of  $n_f = 1.45$  and  $4 \mu\text{m}$  diameter. Before entering the  
110 UHV system, the light passes a 3 dB beam splitter, where it is divided into two beams with almost  
111 identical power. The first part is directed to a power meter for control purposes, while the second  
112 part is guided to the interferometer in the UHV [11]. The fiber end in the interferometer is care-  
113 fully cleaved to achieve high optical quality for the dielectric/vacuum interface having a reflectivity  
114 of  $R_f = 0.04$ . The fourth end of the 3 dB coupler is connected to the detector that is a photore-  
115 ceiver (model HBPR-200M-30K-SI-FC, FEMTO Messtechnik, Berlin, Germany) converting the  
116 incoming light power into a voltage signal. The photoreceiver allows for high sensitivity low-noise  
117 measurements of DC and AC signals with a bandwidth of 200 MHz.

118 The interferometer is precisely aligned via a tube piezo controlled by the R9 control system (RHK  
119 Technology Inc., Troy, MI, USA). Cantilever excitation with a sine wave voltage with a well-  
120 defined amplitude  $V_{exc}$  and overall experiment control is accomplished by a HF2LI (Zurich In-  
121 struments, Zürich, Switzerland). Experiments are performed with the freely oscillating cantilever.  
122 Therefore, the cantilever excitation frequency  $f_{exc}$  is set to the eigenfrequency of the cantilever that

123 is determined by taking a resonance curve before each experiment. By temperature stabilisation of  
 124 the laboratory and the scan head, care is taken to avoid any thermal drift of the cantilever eigenfre-  
 125 quency that might compromise measurements. A model MDO3000 oscilloscope (Tektronix Inc.,  
 126 Beaverton, OR, USA) is used to record the AC output signal of the photoreceiver  $V_{sig}$  that is a volt-  
 127 age between 0 and 10 mV<sub>pp</sub> with a typical noise level of less than 150  $\mu$ V<sub>RMS</sub>. Time traces with a  
 128 length of 4  $\mu$ s at a sampling rate of 250 MS/s are taken and quantised with a resolution of 10 bits.  
 129 Each experiment comprises a set of 20 to 30 measurements with the excitation voltage amplitude  
 130  $V_{exc}$  ramped from 0 to 7 V. This voltage is reduced by a 100:1 voltage divider before it is applied  
 131 to the excitation piezo. For each amplitude, 512 traces of  $V_{sig}$  are taken and averaged, where the  
 132 start of sampling is triggered by the zero crossing of the low noise sinusoidal cantilever excitation  
 133 voltage signal recorded on the second oscilloscope channel.  
 134 For data evaluation, a simplified form of Eq. (5) is fitted to the averaged trace for each amplitude.  
 135 In the fit function of Eq. (6) linearly depending parameters are gathered into one

$$136 \quad V_{sig} = V_{DC} + V_0 \sin\left(\frac{4\pi}{\lambda} (D - A \sin(2\pi f_s t - \varphi)) - \frac{\pi}{2}\right), \quad (6)$$

137 where  $V_{DC}$  represents the constant part of the interferometer signal voltage,  $V_0$  the voltage ampli-  
 138 tude of the interference signal oscillation,  $D = d_0 + d_{err} - q_s$  the actual distance of the center of os-  
 139 cillation from the fiber end,  $f_s$  the frequency reference to the time base of the oscilloscope and  $\varphi$  a  
 140 phase factor covering any phase shift introduced by the electronics in the signal path. The time de-  
 141 pendence of  $S_{loss}$  is neglected, as it is of minute influence for the amplitudes used here. However,  
 142 for experiments with a very large amplitude, this is expected to influence the interference signal.  
 143 We find, that Eq. (6) fits the experimental data for all amplitudes perfectly, as demonstrated for  
 144 one example in Fig. 3. However, for lower amplitudes, the fit does not yield physically meaningful  
 145 results due to the mutual dependence of the parameters  $V_0$ ,  $A$  and  $\varphi$ . We find, for instance, that the  
 146 fit value of  $V_0$  exhibits a dependence on  $V_{exc}$ , while it is evident from Eq. (5) that  $V_0$  should be a  
 147 constant solely determined by system parameters. To yield the correct value  $V_0^{lim}$ , we plot the peak-  
 148 to-peak amplitude  $V_{pp}$  of the  $V_{sig}$  fit curve (see Fig. 3) as a function of  $V_{exc}$  as shown in Fig. 4. We

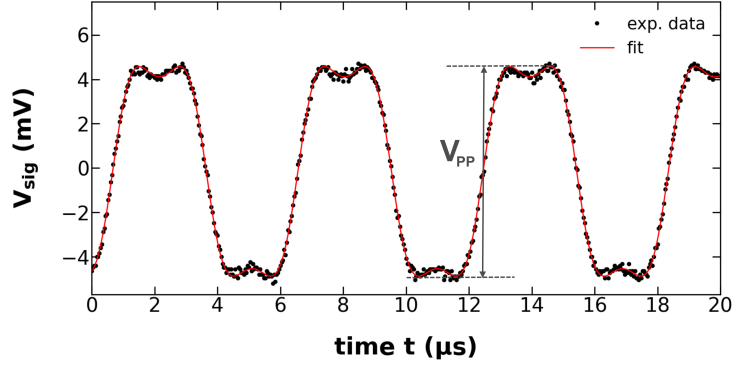


**Figure 3:** Fit of the model for the interferometer signal voltage according to Eq.(6) to experimental data. The cantilever excitation piezo voltage amplitude is  $V_{exc} = 4.25V$  corresponding to an amplitude  $A=86.61$  nm.

149 find that  $V_{pp}$  first rises with amplitude and then saturates at the amplitude limit  $2V_0^{lim}$ . A parameter  
 150 that can reliably be deduced from the fit is  $f_s$  as this is the characteristic fundamental frequency  
 151 of the signal. In the second step of data evaluation, we perform a fit of the same fit function to the  
 152 same experimental data, however, with a reduced number of fit parameters. In this fit,  $V_0^{lim}$  and  
 153  $f_s$  are taken over as fixed values from the first fit, while the other parameters are treated as free fit  
 154 parameters. This two-step procedure allows to determine all signal parameters with high accuracy.

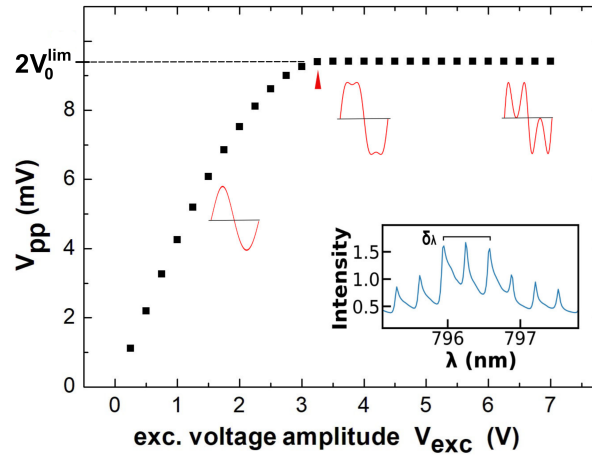


**Figure 4:** Peak-to-peak amplitude  $V_{pp}$  of  $V_{sig}$  (see Fig. 3) as a function of the cantilever excitation voltage amplitude  $V_{exc}$ . The insets show three typical waveforms for  $I_M(t)$  ( $V_{exc}=1.75$  V, 4 V and 7 V) and the central part of the laser diode mode spectrum.

155 As the interferometric method is perfectly suited for the calibration of the cantilever oscillation

156 amplitude, we exemplify the fit procedure and accuracy limits for the fit parameter  $A$ . Amplitude  
 157 calibration means to relate the cantilever oscillation amplitude  $A$  to the voltage  $V_{exc}$  to yield the  
 158 calibration factor  $S = A/V_{exc}$  [14]. An accurate calibration is essential for quantitative NC-AFM  
 159 and, therefore, various methods have been suggested to determine the calibration factor [10,18-21].  
 160 There is a simple and rough, but commonly used method of calibration of the cantilever displace-  
 161 ment by an interferometer, that is based on the measurement shown in Fig. 4. This method uses  
 162 just the data point for the excitation amplitude  $V_{exc}(A = \lambda/8)$ , where saturation in  $V_{pp}$  occurs in-  
 163 dicating that the oscillation exactly covers one fringe with  $-\lambda/8 \leq q \leq +\lambda/8$ . For the experiment  
 164 discussed here, such calibration yields  $S = 20.38$  nm/V. However, from Fig. 4 it is clear that the  
 165 precision of this value is limited as the  $\lambda/8$  point is not well defined.

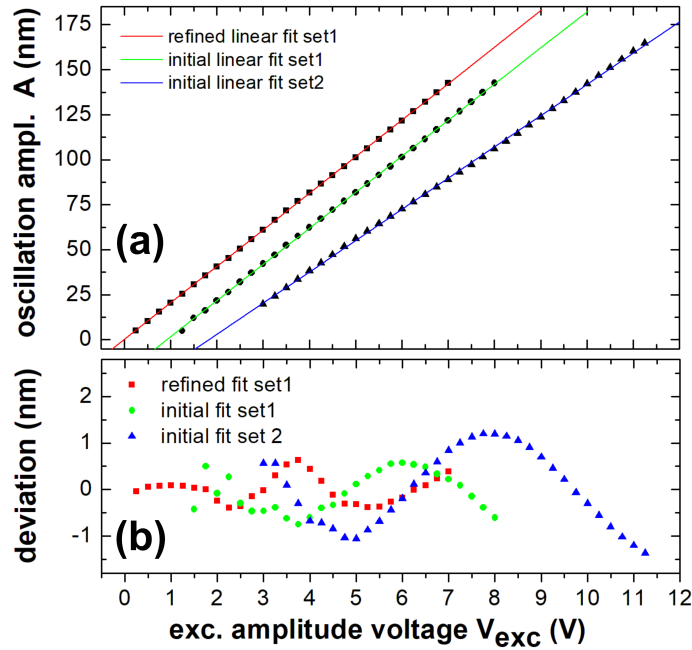


**Figure 5:** (a) The cantilever oscillation amplitude  $A$  is derived from the linear fit of Eq. (6) to experimental time traces  $V_{sig}(t)$  as a function of the excitation voltage amplitude  $V_{exc}$  (squares, circles, triangles). Straight lines are linear fits of  $A(V_{exc})$  data. (b) Residuals of the oscillation amplitudes with respect to the linear fit. Note, that the green and blue data are shifted by 1V along the x axis for better visibility of the graphs.

166 Figure 5 illustrates the enhancement in accuracy that can be achieved by applying the two-step fit  
 167 procedure for data analysis. In this plot of  $A(V_{exc})$ , measurements taken at all amplitudes are in-

168 cluded and fitted by a straight line. The green and blue curves represent measurements taken over  
 169 two days, where the optical fiber has slightly been re-adjusted in between the measurements. The  
 170 curves (circle and triangle) represent data analysed by a single fit, where the green curve represents  
 171 the same data as those shown in Fig. 4. Both measurements yield a linear behaviour, however, with  
 172 a somewhat different slope and, therefore, different calibration factors, which is due to the fiber re-  
 173 adjustment. The residuals plotted in the lower part of the figure demonstrate that measurements are  
 174 free of any significant noise [22], however, we find a smooth undulation of the experimental val-  
 175 ues around zero that stems from the residual mutual dependence of fit parameters. The red curve  
 176 (squares) represents fit results for the data from the green curve treated with the two-step proce-  
 177 dure. The analysis of the residuals reveals that the second step of data processing significantly re-  
 178 duces, but cannot fully remove the undulation.

179 At first sight, the undulation as a systematic error appears as the major limitation for the accuracy  
 180 in determining the calibration factor  $S$ . An extended analysis of several sets of data covering a large  
 181 range of amplitudes yields, however, that the effect of the undulation can be reduced to a negligible  
 182 effect by a proper choice of the analysed range of amplitudes. This is achieved by restricting the  
 183 analysis to a range of amplitudes, where the undulating behaviour yields a compensation of positive  
 184 and negative deviations from the straight line. To obtain limits for the precision and accuracy of the  
 185 result for the amplitude calibration factor, we consider four contributions to the error in  $S$  that are  
 186 expressed in the following formula of error propagation for the linear fit [23]

$$187 \quad \delta_S = S \sqrt{\left(\frac{\delta_{V_{exc}}}{V_{exc}}\right)^2 + \left(\frac{\delta_A}{A}\right)^2 + \left(\frac{\delta_\lambda}{\lambda}\right)^2 + \left(\frac{\delta_{l_c}}{l_c}\right)^2}, \quad (7)$$

188 where  $\delta_{V_{exc}}/V_{exc} = 0.010$  is the excitation voltage output uncertainty according to the HF2 spec-  
 189 ification taken as systematic error of device and  $\delta_A/A = 0.0004$  is the mean of the residuals in  $A$   
 190 divided by the mean value of  $A$ , determined as a oscillation amplitude error. The relative error in  
 191 the wavelength measurement is  $\delta_\lambda/\lambda = 0.00075$ , as discussed below, and the relative error in the  
 192 adjustment of the light spot on the cantilever with length  $l_c$  as indicated in Fig. 1. The positioning

193 error  $\delta_{l_c}$  is estimated from visual inspection of a CCD camera image of the fiber-cantilever gap.  
 194 To estimate the wavelength error  $\delta_\lambda$ , we performed a careful measurement of the laser diode light  
 195 wavelength  $\lambda$  with a spectrograph (Acton series SP-2500i-2556, Princeton Instruments, USA) that  
 196 has been calibrated by 40 atomic lines distributed over the entire visible spectrum to yield an accu-  
 197 rate value for the wavelength at a spectral resolution of 0.050 nm. As evident from the multimode  
 198 spectrum of the laser diode light source shown in the inset of Fig. 4, the spectrum is dominated  
 199 by three modes with a center at the vacuum wavelength  $\lambda = 796.49$  nm. Assuming that interfer-  
 200 ence occurs in the optical fiber, we calculate the laser wavelength in the fiber with  $n = 1.45$  as  
 201  $\lambda_f = 549.24$  nm for oscillation amplitude calibration. We take the spectral distance of the two  
 202 neighboring lines as a conservative estimate for the wavelength error  $\delta_\lambda = 0.60$  nm. Note, that  
 203 the errors  $\delta_{V_{exc}}$  and  $\delta_A$  are not independent variables. We treat them separately as  $\delta_{V_{exc}}$  is a statisti-  
 204 cal error, while  $\delta_A$  represents an additional systematic error due to the residuals in the linear fit of  
 205  $A(V_{exc})$ . Taking these error margins into account, we yield the final result for the amplitude cali-  
 206 bration factor  $S = (20.299 \pm 0.050)$  nm/V.

207 In summary, we derived a model for the description of the time domain signal of a Michelson-  
 208 type interferometer used to measure the displacement of a (quasi) harmonically oscillating micro-  
 209 cantilever in an NC-AFM. The analysis demonstrates that the interferometer signal is a non-trivial  
 210 function of the cantilever excitation, where increasing excitation amplitude is translated into in-  
 211 creasing non-linearity and complexity of the response signal. A fit of the derived response func-  
 212 tion to experimental data yields excellent results for all system parameters. However, care has to be  
 213 taken to minimise systematic errors resulting from the mutual dependence of fit parameters. The  
 214 method specifically allows to determine the cantilever oscillation amplitude calibration factor with  
 215 a remarkable 0.15% relative error.

216 The strength of the interferometric calibration is the high accuracy that can be achieved as the cal-  
 217 ibration of the amplitude can be traced to the light wavelength, which can be most precisely and  
 218 accurately measured. The error analysis shows, that the weakest point is the accurate positioning  
 219 of the light beam at the position of the tip that is relevant for NC-AFM measurements. In experi-

220 ments, as introduced here, noise is not a limiting factor for the quantitative evaluation of the inter-  
221 ferometric signal and there is headroom left for improvement by optimising the experimental setup.

## 222 **References**

- 223 1. Yang, S. M.; Zhang, G. F. *Measurement Science and Technology* **2018**, *29*, 102001.
- 224 2. Bond, C.; Brown, D.; Freise, A.; Strain, K. A. *Living Reviews in Relativity* **2016**, *19*, 3.
- 225 3. Buikema, A.; et al., *Physical Review D* **2020**, *102*, 062003.
- 226 4. Heinze, J.; Danzmann, K.; Willke, B.; Vahlbruch, H. *Physical Review Letters* **2022**, *129*,  
227 031101.
- 228 5. Rugar, D.; Mamin, H. J.; Erlandsson, R.; Stern, J. E.; Terris, B. D. *Review of Scientific Instru-*  
229 *ments* **1988**, *59*, 2337.
- 230 6. Hoogenboom, B. W.; Frederix, P. L. T. M.; Yang, J. L.; Martin, S.; Pellmont, Y.;  
231 Steinacher, M.; Zäch, S.; Langenbach, E.; Heimbeck, H.-J.; Engel, A.; Hug, H. J. *Review of*  
232 *Scientific Instruments* **2005**, *86* (074101), 3.
- 233 7. Hoogenboom, B. W.; Frederix, P. L. T. M.; Fotiadis, D.; Hug, H. J.; Engel, A. *Nanotechnology*  
234 **2008**, *19*, 384019.
- 235 8. Morita, K.; Sugimoto, Y.; Sasagawa, Y.; Abe, M.; Morita, S. *Nanotechnology* **2010**, *21*,  
236 305704.
- 237 9. Karci, O.; Dede, M.; Oral, A. *Review of Scientific Instruments* **2014**, *85*, 103705.
- 238 10. Çelik, U.; Karci, O.; Uysallı, Y.; Özer, H. O.; Oral, A. *Review of Scientific Instruments* **2017**,  
239 *88*, 013705.
- 240 11. v. Schmidfeld, A.; Nörenberg, T.; Temmen, M.; Reichling, M. *Beilstein J. Nanotechnol.* **2016**,  
241 *7*, 841.

- 242 12. v. Schmidfeld, A.; Reichling, M. *Applied Physics Letters* **2015**, *107*, 123111.
- 243 13. Söngen, H.; Bechstein, R.; Kühnle, A. *Journal of Physics: Condensed Matter* **2017**, *29*,  
244 274001.
- 245 14. Rahe, P.; Heile, D.; Olbrich, R.; Reichling, M. *Beilstein J. Nanotechnol.* **2022**, *13*, 610.
- 246 15. Tröger, L. *Aufbau eines Tieftemperatur-Rasterkraftmikroskopes*; Sierke Verlag, 2009.
- 247 16. Drevniok, B.; Paul, W. M. P.; Hairsine, K. R.; McLean, A. B. *Review of Scientific Instruments*  
248 **2012**, *83*, 033706.
- 249 17. Moheiman, S. O. R. *Review of Scientific Instruments* **2008**, *79*, 071101.
- 250 18. Simon, G. H.; Heyde, M.; Rust, H.-P. *Nanotechnology* **2007**, *18*, 255503.
- 251 19. Sugimoto, Y.; Nakajima, Y.; Sawada, D.; Morita, K.; Abe, M.; Morita, S. *Physical Review B*  
252 **2010**, *81*, 245322.
- 253 20. Martínez, J. F. G.; Nieto-Carvajal, I.; Colchero, J. *Nanotechnology* **2013**, *24*, 185701.
- 254 21. Dagdeviren, O. E.; Miyahara, Y.; Mascaro, A.; Grütter, P. *Review of Scientific Instruments*  
255 **2019**, *90*, 013703.
- 256 22. Lübbe, J.; Temmen, M.; Rode, S.; Rahe, P.; Kühnle, A.; Reichling, M. *Beilstein Journal of*  
257 *Nanotechnology* **2013**, *4*, 32.
- 258 23. Hughes, I. G.; Hase, T. P. A. *Measurements And Their Uncertainties*; Oxford University Press,  
259 2009.